Journal of Materials Chemistry C

ROYAL SOCIETY OF CHEMISTRY

COMMUNICATION

View Article Online
View Journal | View Issue

Cite this: J. Mater. Chem. C, 2023, 11, 10149

Received 30th April 2023,
Accepted 8th July 2023

DOI: 10.1039/d3tc01520c

rsc.li/materials-c

A nonbenzenoid acepleiadylene derivative with small band gap for near-infrared organic phototransistors†

Pengcai Liu,‡ Lin Fu,‡ Xiao-Yu Tang, Rui Xue, Lijuan Zhang, Jiawen Cao and Xiao-Ye Wang *

Near-infrared (NIR) materials have attracted intensive attention in recent years. In this paper, we design a new nonbenzenoid acepleiadylene derivative (APD-DPP) with NIR absorption by taking advantage of the narrow band gap of acepleiadylene. Experimental and theoretical studies show that APD-DPP has strong NIR absorption and a high carrier mobility of up to 0.30 $cm^2 V^{-1} s^{-1}$. NIR phototransistors based on APD-DPP exhibit a high photoresponsivity of 1.30 A W^{-1}, a photosensitivity of 1.34×10^4, and a specific detectivity of 5.31×10^{11} Jones. These results reveal the potential of APD as a building block for NIR-absorbing materials.

Near-infrared (NIR) materials have attracted intensive attention in recent years due to the wide applications of NIR light (700–1700 nm)[1,2] in the fields of medical monitoring, quality inspection, biological imaging *etc.*[2–9] In particular, NIR phototransistors can convert NIR light into electrical signals, realizing the detection of NIR light.[10–17] Traditional NIR phototransistors are mainly based on inorganic semiconductor materials, which nevertheless have the disadvantages of high cost and temperature sensitivity.[18] Benefiting from the characteristics of light weight, flexibility and solution processibility, organic semiconductors are ideal candidates for NIR light detection.[19–26] For high-performance NIR organic phototransistors (OPTs), organic materials with both strong NIR absorption and high carrier mobility are required.[13,16] However, these kinds of materials are rarely reported, which hinders the development of NIR OPTs. The common design strategy for NIR-absorbing materials mainly involves increasing the conjugation length and constructing donor (D) and acceptor (A) alternating structures.[27–29] Compared with the complicated synthetic routes of enlarging the conjugation length, the D–A alternating structures feature concise synthetic routes and adjustable energy levels using different building blocks.[30] Besides the NIR absorption, D–A alternating structures have strong intermolecular interactions induced by the tight π–π stacking and electrostatic interaction, which are conducive to charge transport.[31,32] Although some studies on D–A type organic semiconductors in NIR photodetectors have been reported before,[30,33–39] there are few examples that can achieve high NIR OPT performance.

Nonbenzenoid polycyclic arenes contain nonhexagon rings in a polycyclic aromatic system.[40–42] The attention on these molecules with structural diversity has been boosted during the past decade,[43–46] especially in the fields of organic field-effect transistors (OFETs),[47,48] magnetic materials,[49,50] thermoelectrics,[51] sensing,[52] and solar cells.[53] Acepleiadylene (APD), one of the nonbenzenoid isomers of pyrene, features a narrower energy gap between the highest occupied molecular orbital (HOMO) and the lowest unoccupied molecular orbital (LUMO), a larger molecular dipole moment, and a separated charge distribution (Fig. 1a and b).[54] Consequently, APD has great potential to be

State Key Laboratory of Elemento-Organic Chemistry, Frontiers Science Center for New Organic Matter, College of Chemistry, Nankai University, Weijin Road 94, Tianjin 300071, China. E-mail: xiaoye.wang@nankai.edu.cn

† Electronic supplementary information (ESI) available. See DOI: https://doi.org/10.1039/d3tc01520c

‡ These authors contributed equally to this work.

Xiao-Ye Wang

Xiao-Ye Wang received his BSc degree from Nankai University in 2009 and obtained his PhD degree from Peking University in 2014 under the supervision of Prof. Jian Pei. From 2014 to 2019, he was a postdoctoral researcher and a Humboldt Fellow in the group of Prof. Klaus Müllen at the Max Planck Institute for Polymer Research in Germany. In 2019, he moved to Nankai University to start his independent research as a professor of Chemistry. His research focuses on organic and nanocarbon materials for optoelectronic applications.

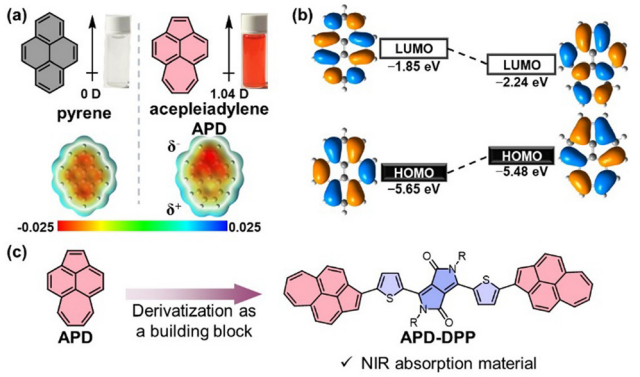

Fig. 1 (a) Comparison of pyrene and acepleiadylene (APD) with the molecular dipole moment, colour in solution, and electrostatic potential (ESP) diagram. (b) Frontier molecular orbitals (FMO) and energy levels of pyrene and APD. (c) Design strategy of the novel NIR-absorbing material **APD-DPP** combining the nonbenzenoid building block APD and the D–A–D structure.

applied in optoelectronic materials as a building block. Considering the narrow HOMO–LUMO gap of APD, here we design and synthesize an APD derivative (**APD-DPP**) with APD as the donor moieties and diketopyrrolopyrrole (DPP) as the acceptor moiety, which can achieve NIR absorption (Fig. 1c). Taking advantage of both the high charge carrier mobility and the NIR absorption character of **APD-DPP**, NIR phototransistors based on **APD-DPP** have been fabricated, revealing high device performance.

The synthetic routes to **APD-DPP** and its benzenoid counterparts are shown in Scheme 1. From known precursor **1**,[55] **APD-DPP** was obtained using the Suzuki–Miyaura coupling in a yield of 64%. Following a similar synthetic strategy, **1Py-DPP** and **2Py-DPP** were also synthesized in 38% and 42% yields, respectively. The structures of all these compounds were identified by ^{1}H and ^{13}C NMR spectroscopies and high-resolution mass spectrometry (HRMS).

In order to prove the advantage of APD in the absorption of long-wavelength photons, the UV-Vis absorption spectra in both toluene solutions and thin films were recorded (Fig. 2). The three molecules show a similar absorption band at the wavelength from 300 to 500 nm in toluene solution. These high

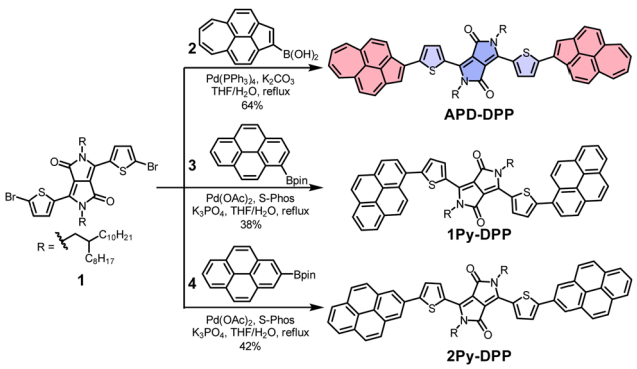

Scheme 1 Synthetic routes to **APD-DPP**, **1Py-DPP**, and **2Py-DPP**.

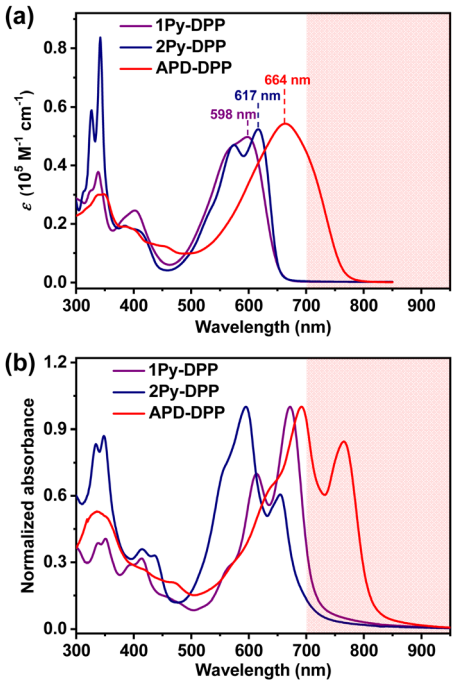

Fig. 2 The UV-Vis absorption spectra of **1Py-DPP**, **2Py-DPP**, and **APD-DPP** (a) in toluene solutions (1×10^{-5} M) and (b) in thin films.

energy absorption bands stem from the donor and acceptor moieties by comparing the absorption spectra of **APD-DPP**, **1Py-DPP**, and **2Py-DPP** with their corresponding building blocks (Fig. S2, ESI†). The low-energy absorption bands (500–800 nm) are assigned to the intramolecular charge transfer (ICT) bands. **APD-DPP** exhibits a more red-shifted absorption maximum (664 nm) than **1Py-DPP** (598 nm) and **2Py-DPP** (617 nm), which results from the stronger ICT effect, implying that APD is a stronger electron donor than pyrene given that acceptors are the same DPP segment. Besides, the ICT band of **APD-DPP** reaches the NIR region, while its benzenoid isomers do not. Additionally, there is an obvious red-shift of the absorption maximum by ~100 nm in thin films as compared with those in solution for all three molecules. As a result, the absorption spectrum of **APD-DPP** covers more NIR region ranging from 700 to 900 nm, while the other two counterparts still cannot reach the NIR region. Based on the electrochemical measurements (Fig. S4, ESI†), **APD-DPP** exhibits a higher HOMO energy level (−5.53 eV for **APD-DPP**, −5.76 eV for **1Py-DPP**, and −5.74 eV for **2Py-DPP**) and a lower LUMO energy level (−4.02 eV for **APD-DPP**, −3.85 eV for **1Py-DPP**, and −3.86 eV for **2Py-DPP**) compared with its benzenoid isomers, presumably owing to the stronger intramolecular interaction between APD and DPP moieties. The resulting narrow HOMO–LUMO gap of **APD-DPP** proves the capability of APD in tuning frontier molecular orbital (FMO) energy levels.

To further clarify the reason for the small band gap of **APD-DPP**, theoretical calculations were conducted (Fig. 3). Time-dependent density functional theory (TD-DFT) calculations illustrate that the lowest-energy transition of $S_0 \rightarrow S_1$ in all these three molecules is mainly attributed to the HOMO → LUMO

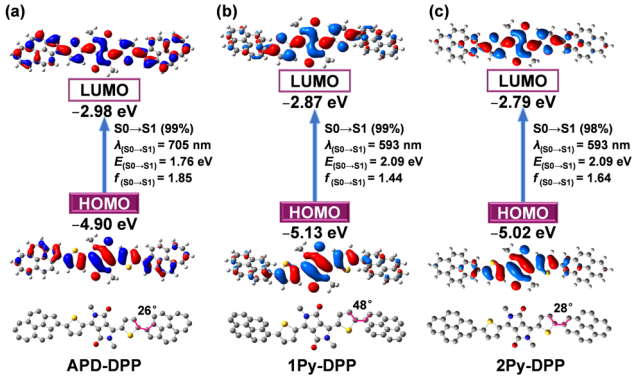

Fig. 3 Calculated molecular conformations, the HOMO and LUMO distributions, energy levels, and the $S_0 \rightarrow S_1$ transition analyses of (a) **APD-DPP**, (b) **1Py-DPP**, and (c) **2Py-DPP**.

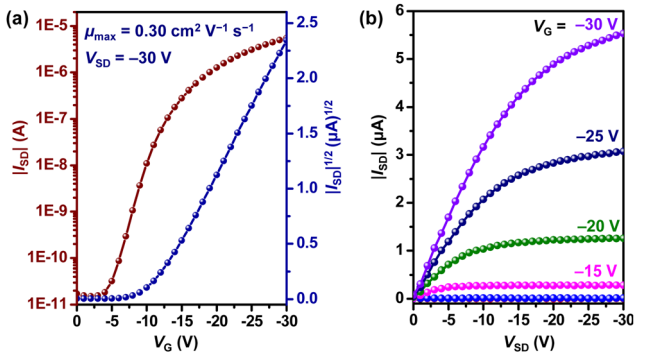

Fig. 4 Typical transfer (a) and output (b) curves of OFET devices based on **APD-DPP** thin films.

transition with strong oscillator strengths (1.85 for **APD-DPP**, 1.44 for **1Py-DPP**, and 1.64 for **2Py-DPP**), corresponding to the large molar extinction coefficients at the absorption maxima (54279 M^{-1} cm^{-1} for **APD-DPP**, 52348 M^{-1} cm^{-1} for **1Py-DPP**, and 49748 M^{-1} cm^{-1} for **2Py-DPP**) in solution. The transition energy of **APD-DPP** was calculated as 1.76 eV, corresponding to an absorption peak at 705 nm, which is more red-shifted compared with those of **1Py-DPP** and **2Py-DPP**. Additionally, the FMO distribution of **APD-DPP** is more delocalized, implying better conjugation between APD and DPP moieties, which leads to a stronger intramolecular interaction in **APD-DPP** than those in **1Py-DPP** and **2Py-DPP**. A smaller dihedral angle of 26° is observed between APD and thiophene moieties for **APD-DPP** than those for **1Py-DPP** (48°) and **2Py-DPP** (28°) based on the optimized geometries, which is also in favour of the intramolecular conjugation between APD and DPP segments. Both the experimental data and the calculated results prove that APD has a vital effect on the energy levels as well as the absorption feature, which indicates the potential of APD as a building block in NIR-absorption materials.

To investigate the charge transport properties of **APD-DPP**, bottom-gate top-contact OFET devices were fabricated by spin-coating a solution of **APD-DPP** in trichloroethylene onto 12-cyclohexyldodecylphosphonic acid (CDPA)-modified AlO_x/SiO_2/Si substrates. Meanwhile, the charge transport properties of two benzenoid isomers **1Py-DPP** and **2Py-DPP** were also characterized for comparison. All three molecules show hole transport characteristics and their OFET characterization data are summarized in Table S2 (ESI†). For optimizing the device performance, different annealing temperatures were applied on these thin films. The mobility of the OFET devices based on the **APD-DPP** films gradually increases from 0.036 cm^2 V^{-1} s^{-1} to 0.30 cm^2 V^{-1} s^{-1} when the annealing temperature increases from 60 °C to 150 °C. However, as the annealing temperature further increases to 160 °C, the mobility decreases to 0.08 cm^2 V^{-1} s^{-1} due to the film melting or deformation. Therefore, the optimized annealing temperature of **APD-DPP** is 150 °C, while the optimized annealing temperature of **1Py-DPP** and **2Py-DPP** is 90 °C. These results indicate that the OFET device of **APD-DPP** has a better thermal stability. Importantly, **APD-DPP** has the best charge transport performance among these three molecules and its maximum mobility is 0.30 cm^2 V^{-1} s^{-1}, which is larger than the highest mobilities of **1Py-DPP** (2.60×10^{-3} cm^2 V^{-1} s^{-1}) and **2Py-DPP** (6.38×10^{-2} cm^2 V^{-1} s^{-1}). The transfer and output curves of **APD-DPP**-based OFET devices are shown in Fig. 4. It can be concluded that **APD-DPP** has an advantage over its benzenoid isomers in charge transport. Because the transport speed of dissociated photoinduced excitons directly affects the intensity of the photocurrent, the charge transport performance is vital to photodetection in NIR OPTs.

Combining the better charge transport properties and the NIR absorption of **APD-DPP**, we used **APD-DPP** as the active layer in NIR OPTs. To optimize the OPT performance, a commonly used electron blocking layer MoO_3 was introduced into the original OFET device structure (Fig. 5a). The performance measurements were carried out in the dark and under illumination using a 730 nm light-emitting diode (LED) with

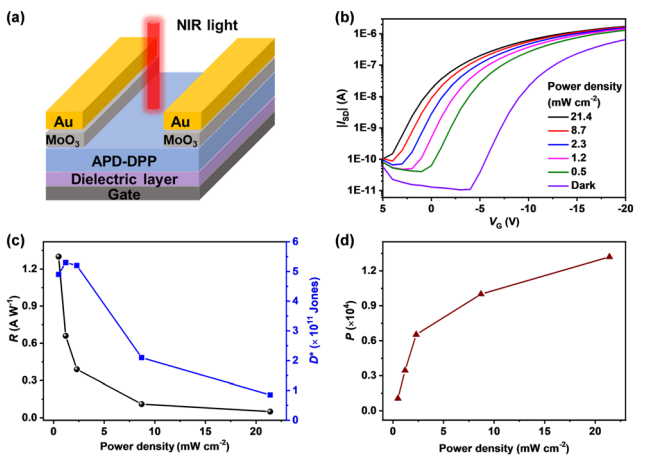

Fig. 5 NIR-responsive characteristics of the OPT devices with **APD-DPP** as the channel layer. (a) Schematic diagram of the NIR phototransistor. (b) Transfer curves (V_{SD} = −20 V) under different illumination intensities of NIR light (λ = 730 nm). (c), (d) The values of R, D^* and P under different illumination intensities (λ = 730 nm, V_{SD} = −20 V, V_G = −20 V for R, V_G = −4 V for D^* and P).

adjustable light intensity. It is observed that the introduction of electron blocking layer MoO_3 significantly improves the NIR light detection performance of the OPT devices (Fig. S9, S10 and Tables S3, S4, ESI†). Fig. 5b shows the transfer curves of the OPT device in the dark and under different illumination intensities. As the illumination intensity increases from 0.5 mW cm^{-2} to 21.4 mW cm^{-2}, the source-drain current (I_{SD}) increases gradually due to the extra photogenerated current under the illumination of NIR light and the device shows a good NIR light detection performance. Fig. 5c shows the tendency of photoresponsivity (R) and specific detectivity (D^*) under 730 nm light at different illumination intensities. With the increase of the illumination intensity, both the values of R and D^* show a similar downward trend. The R reaches the maximum value of 1.30 A W^{-1} when the illumination intensity is 0.5 mW cm^{-2} at V_G of −20 V, while the D^* reaches the maximum value of 5.31×10^{11} Jones when the illumination intensity is 1.2 mW cm^{-2} at V_G of −4 V. The photosensitivity (P) increases as the illumination intensity is enhanced (Fig. 5d). When the illumination intensity reaches 21.4 mW cm^{-2}, the maximum P value is 1.34×10^4. The NIR phototransistor performance data are summarized in Table S3 (ESI†). In this device configuration, the maximum photoresponsivity, photosensitivity, and specific detectivity are R_{max} = 1.30 A W^{-1}, P_{max} = 1.34×10^4, and $D^*_{max} = 5.31 \times 10^{11}$ Jones. Compared with the reported single-component thin-film NIR OPTs (Table S5, ESI†), the performance of **APD-DPP** is among the best NIR OPT devices.

In summary, we have designed and synthesized a new nonbenzenoid APD derivative **APD-DPP** with NIR absorption by taking advantage of the narrow band gap and strong electron-donating effect of APD. Experimental and theoretical studies show that **APD-DPP** has a narrower band gap than its benzenoid isomers **1Py-DPP** and **2Py-DPP**, with the absorption extending to the NIR region. Additionally, higher carrier mobility is observed for **APD-DPP** (0.30 cm^2 V^{-1} s^{-1}) as compared with its benzenoid isomers (10^{-3}–10^{-2} cm^2 V^{-1} s^{-1} for **1Py-DPP** and **2Py-DPP**). Furthermore, NIR phototransistors based on **APD-DPP** have been fabricated, exhibiting photoresponsivity of 1.30 A W^{-1}, photosensitivity of 1.34×10^4, and specific detectivity of 5.31×10^{11} Jones. These results indicate the potential of APD as a building block for NIR materials and demonstrate the value of nonbenzenoid polycyclic arenes for optoelectronic applications.

Conflicts of interest

There are no conflicts to declare.

Acknowledgements

We are grateful for the financial support from the National Natural Science Foundation of China (No. 92256304 and 22071120), the National Key R&D Program of China (2020YFA0711500), and the Fundamental Research Funds for the Central Universities.

Notes and references

1 G. Hong, A. L. Antaris and H. Dai, *Nat. Biomed. Eng.*, 2017, **1**, 0010.
2 S. He, J. Song, J. Qu and Z. Cheng, *Chem. Soc. Rev.*, 2018, **47**, 4258–4278.
3 J. Li and K. Pu, *Chem. Soc. Rev.*, 2019, **48**, 38–71.
4 C. Yan, Y. Zhang and Z. Guo, *Coord. Chem. Rev.*, 2021, **427**, 213556.
5 C. Liu, K. Wang, X. Gong and A. J. Heeger, *Chem. Soc. Rev.*, 2016, **45**, 4825–4846.
6 P. Reineck and B. C. Gibson, *Adv. Opt. Mater.*, 2017, **5**, 1600446.
7 B. Xie, Z. Chen, L. Ying, F. Huang and Y. Cao, *InfoMat*, 2020, **2**, 57–91.
8 B. Pigulski, K. Shoyama and F. Würthner, *Angew. Chem., Int. Ed.*, 2020, **59**, 15908–15912.
9 Q. Zhou, J. Yang, M. Du, X. Yu, C. Li, X.-S. Zhang, Q. Peng, G. Zhang and D. Zhang, *J. Mater. Chem. C*, 2022, **10**, 2814–2820.
10 X. Gong, M. Tong, Y. Xia, W. Cai, J. S. Moon, Y. Cao, G. Yu, C.-L. Shieh, B. Nilsson and A. J. Heeger, *Science*, 2009, **325**, 1665–1667.
11 J. Huang, J. Lee, J. Vollbrecht, V. V. Brus, A. L. Dixon, D. X. Cao, Z. Zhu, Z. Du, H. Wang, K. Cho, G. C. Bazan and T.-Q. Nguyen, *Adv. Mater.*, 2020, **32**, 1906027.
12 J. H. Kim, A. Liess, M. Stolte, A.-M. Krause, V. Stepanenko, C. Zhong, D. Bialas, F. Spano and F. Würthner, *Adv. Mater.*, 2021, **33**, 2100582.
13 D. Zhu, D. Ji, L. Li and W. Hu, *J. Mater. Chem. C*, 2022, **10**, 13312–13323.
14 T. Han, Z. Wang, N. Shen, Z. Zhou, X. Hou, S. Ding, C. Jiang, X. Huang, X. Zhang and L. Liu, *Nat. Commun.*, 2022, **13**, 1332.
15 B. Yang, Y. Wang, L. Li, J. Zhang, J. Wang, H. Jiao, D. Hao, P. Guo, S. Zeng, Z. Hua and J. Huang, *Adv. Funct. Mater.*, 2021, **31**, 2103787.
16 C. Wang, X. Zhang and W. Hu, *Chem. Soc. Rev.*, 2020, **49**, 653–670.
17 N. Li, Z. Lan, L. Cai and F. Zhu, *J. Mater. Chem. C*, 2019, **7**, 3711–3729.
18 K.-J. Baeg, M. Binda, D. Natali, M. Caironi and Y.-Y. Noh, *Adv. Mater.*, 2013, **25**, 4267–4295.
19 D. Li, J. Du, Y. Tang, K. Liang, Y. Wang, H. Ren, R. Wang, L. Meng, B. Zhu and Y. Li, *Adv. Funct. Mater.*, 2021, **31**, 2105887.
20 J. Zhong, X. Wu, S. Lan, Y. Fang, H. Chen and T. Guo, *ACS Photonics*, 2018, **5**, 3712–3722.
21 G. Wang, K. Huang, Z. Liu, Y. Du, X. Wang, H. Lu, G. Zhang and L. Qiu, *ACS Appl. Mater. Interfaces*, 2018, **10**, 36177–36186.
22 Z. Bao and X. Chen, *Adv. Mater.*, 2016, **28**, 4177–4179.
23 Y. Su, X. Ping, K. J. Yu, J. W. Lee, J. A. Fan, B. Wang, M. Li, R. Li, D. V. Harburg, Y. Huang, C. Yu, S. Mao, J. Shim, Q. Yang, P.-Y. Lee, A. Armonas, K.-J. Choi, Y. Yang, U. Paik, T. Chang, T. J. Dawidczyk, Y. Huang, S. Wang and J. A. Rogers, *Adv. Mater.*, 2017, **29**, 1604989.

24 Z. Zhang and Z. Bao, *Natl. Sci. Rev.*, 2023, **10**, nwac093.
25 N. Matsuhisa, X. Chen, Z. Bao and T. Someya, *Chem. Soc. Rev.*, 2019, **48**, 2946–2966.
26 Y. Zhang, Y. Yu, X. Liu, J. Miao, Y. Han, J. Liu and L. Wang, *Adv. Mater.*, 2023, **35**, 2211714.
27 M. Li, C. An, W. Pisula and K. Müllen, *Acc. Chem. Res.*, 2018, **51**, 1196–1205.
28 M. Madhu, R. Ramakrishnan, V. Vijay and M. Hariharan, *Chem. Rev.*, 2021, **121**, 8234–8284.
29 H. Phan, M. Wang, G. C. Bazan and T.-Q. Nguyen, *Adv. Mater.*, 2015, **27**, 7004–7009.
30 H. Son, T. Kim, C. Lee, H. Kim and Y. Kim, *J. Mater. Chem. C*, 2022, **10**, 3951–3958.
31 J. Li, Y. Zhao, H. S. Tan, Y. Guo, C.-A. Di, G. Yu, Y. Liu, M. Lin, S. H. Lim, Y. Zhou, H. Su and B. S. Ong, *Sci. Rep.*, 2012, **2**, 754.
32 Z.-F. Yao, H.-Y. Liu, Z.-Y. Wang, Z.-K. Zhou, J.-Y. Wang and J. Pei, *Chem. – Asian J.*, 2019, **14**, 1686–1691.
33 Y. Cho, T. Kim, W. Lee, H. Kim and Y. Kim, *J. Mater. Chem. C*, 2023, **11**, 2970–2976.
34 J. Park, C. Lee, T. Kim, H. Kim and Y. Kim, *Adv. Electron. Mater.*, 2021, **7**, 2000932.
35 S. Lee, T. Kim, H. Kim and Y. Kim, *ACS Appl. Mater. Interfaces*, 2021, **3**, 6056–6062.
36 S. Kim, D. Lee, J. Lee, Y. Cho, S.-H. Kang, W. Choi, J. H. Oh and C. Yang, *Chem. Mater.*, 2021, **33**, 7499–7508.
37 C. Xiao, C. Li, F. Liu, L. Zhang and W. Li, *J. Mater. Chem. C*, 2020, **8**, 5370–5374.
38 Y. Tang, W. Ge, P. Deng, Q. Zhang, Y. Liao, Z. Xiong, W. Lan, B. Wei and Y. Lei, *J. Mater. Chem. C*, 2020, **8**, 16915–16922.
39 S. Lee, C. Lee, H. Kim and Y. Kim, *J. Mater. Chem. C*, 2020, **8**, 15778–15787.
40 H. Xin, B. Hou and X. Gao, *Acc. Chem. Res.*, 2021, **54**, 1737–1753.
41 J. Huang, S. Huang, Y. Zhao, B. Feng, K. Jiang, S. Sun, C. Ke, E. Kymakis and X. Zhuang, *Small Methods*, 2020, **4**, 2000628.
42 S. H. Pun and Q. Miao, *Acc. Chem. Res.*, 2018, **51**, 1630–1642.
43 Chaolumen, I. A. Stepek, K. E. Yamada, H. Ito and K. Itami, *Angew. Chem., Int. Ed.*, 2021, **60**, 23508–23532.
44 Y.-Y. Huang, B. Wu, D. Shi, D. Liu, W. Meng, J. Ma, L. Qin, C. Li, G. Zhang, X.-S. Zhang and D. Zhang, *Angew. Chem., Int. Ed.*, 2023, **62**, e202300990.
45 J. Wang, F. G. Gámez, J. Marín-Beloqui, A. Diaz-Andres, X. Miao, D. Casanova, J. Casado and J. Liu, *Angew. Chem., Int. Ed.*, 2023, **62**, e202217124.
46 L. Yang, Y.-Y. Ju, M. A. Medel, Y. Fu, H. Komber, E. Dmitrieva, J.-J. Zhang, S. Obermann, A. G. Campaña, J. Ma and X. Feng, *Angew. Chem., Int. Ed.*, 2023, **62**, e202216193.
47 X.-S. Zhang, Y.-Y. Huang, J. Zhang, W. Meng, Q. Peng, R. Kong, Z. Xiao, J. Liu, M. Huang, Y. Yi, L. Chen, Q. Fan, G. Lin, Z. Liu, G. Zhang, L. Jiang and D. Zhang, *Angew. Chem., Int. Ed.*, 2020, **59**, 3529–3533.
48 H. Xin, J. Li, R.-Q. Lu, X. Gao and T. M. Swager, *J. Am. Chem. Soc.*, 2020, **142**, 13598–13605.
49 A. Konishi, K. Horii, D. Shiomi, K. Sato, T. Takui and M. Yasuda, *J. Am. Chem. Soc.*, 2019, **141**, 10165–10170.
50 J. Liu, S. Mishra, C. A. Pignedoli, D. Passerone, J. I. Urgel, A. Fabrizio, T. G. Lohr, J. Ma, H. Komber, M. Baumgarten, C. Corminboeuf, R. Berger, P. Ruffieux, K. Müllen, R. Fasel and X. Feng, *J. Am. Chem. Soc.*, 2019, **141**, 12011–12020.
51 T. Tang, A. K. K. Kyaw, Q. Zhu and J. Xu, *Chem. Commun.*, 2020, **56**, 9388–9391.
52 B. Hou, J. Li, Z. Zhou, W. L. Tan, X. Yang, J. Zhang, C. R. McNeill, C. Ge, J. Wang and X. Gao, *ACS Mater. Lett.*, 2022, **4**, 392–400.
53 H. Xin, C. Ge, X. Jiao, X. Yang, K. Rundel, C. R. McNeill and X. Gao, *Angew. Chem., Int. Ed.*, 2018, **57**, 1322–1326.
54 P. Liu, X.-Y. Chen, J. Cao, L. Ruppenthal, J. M. Gottfried, K. Müllen and X.-Y. Wang, *J. Am. Chem. Soc.*, 2021, **143**, 5314–5318.
55 H. Li, F. Liu, X. Wang, C. Gu, P. Wang and H. Fu, *Macromolecules*, 2013, **46**, 9211–9219.